

PROPULSION/AIRFRAME INTEGRATION CONSIDERING LOW DRAG AND LOW SONIC BOOM

Atsushi UENO*, **Yasushi WATANABE***
* Japan Aerospace Exploration Agency

Keywords: SST, Optimization, Aerodynamic performance, Sonic boom

Abstract


This paper describes a propulsion/airframe integration for a supersonic transport considering low-drag and low-boom. Three types of nacelle layout (i.e., over-wing, under-wing, and side-body nacelles) were considered and the nacelle position was optimized to reduce both drag and sonic boom intensity. Results show the importance of the nacelle shock wave in determining longitudinal and chord-wise nacelle positions that has a larger impact on low-drag and low-boom than span-wise, lateral, and vertical nacelle positions. The Pareto optimal solutions show that the side-body nacelle realizes the optimum compromise between low-drag and low-boom by utilizing the nacelle shock wave. The key point in determining the longitudinal position of side-body nacelles is to obtain the optimum compromise between increase in the angle of attack and decrease in the wind drag, both of which are caused by the nacelle shock wave.

1 Introduction

Japan Aerospace Exploration Agency (JAXA) is promoting a basic research program to realize an economically-viable and environmentally-friendly small supersonic transport [1]. In this program, the technical reference aircraft shown in Table 1 was defined and four technical targets were set: 1) to reduce the structure weight by 15% compared to the Concorde technology, 2) to reduce the sonic boom overpressure by half, 3) to achieve the cruise lift-to-drag ratio (L/D) of higher than 8, and 4) to meet ICAO airport noise regulations.

A low-drag and low-boom design has been extensively studied. At JAXA, the flight test using unmanned aircrafts are conducted to validate its low-drag and low-boom design technology [2]. Most of past studies, however, deal with an airframe alone, and the integration of a propulsion system with an airframe is not fully discussed. The airport noise regulations have a large impact on engine specifications such as bypass ratio and fan diameter, which in turn affects L/D through the skin friction drag of a nacelle and the interference drag between nacelle and airframe. The nacelle shock wave may degrade low-drag and low-boom performance examined with an airframe alone. Thus, the integration of propulsion system and airframe is an important research area in order to realize JAXA's four technical targets.

Table 1. Specification of JAXA QSST

Length	53 m	
Span	23 m	
Weight	70 ton	
Speed	1.6 Mach	
Range	3500 nm	
Passenger	30-50	

JAXA has optimized engine specifications of the technical reference aircraft considering ICAO airport noise regulations as well as range performance [3]. This study revealed that the fan diameter of the engine becomes about 60% of the fuselage diameter in order to reduce the exhaust velocity of the engine. The next step is to integrate this large-sized engine with the airframe considering low-drag and low-boom performance. Several nacelle layouts such as under-wing nacelle [4], over-wing nacelle [5], and side-body nacelle [6] have been studied. At

the moment, however, unified views on design guides for the optimum nacelle layout seems to be not established yet. Thus, our research objective is to derive design guides for the nacelle layout in order to realize low-drag and low-boom performance.

2 Definition of Aerodynamic Shape

Three types of nacelle layout (i.e., over-wing, under-wing, and side-body nacelles) were considered. The nacelle position was optimized for each layout and design guides are discussed to achieve low-drag and low-boom performance.

When a nacelle is integrated into an airframe, a nacelle volume affects the area-ruling that is examined with an airframe alone. Thus, the area-ruling should be reviewed depending on the nacelle position in order to minimize the wave drag. In this study, however, we think the interference drag between nacelle and airframe has a larger impact on L/D than the additional wave drag caused by not reviewing the area-ruling. Thus, the airframe shape was fixed during the optimization. The nacelle shape was also fixed with some exceptions described below.

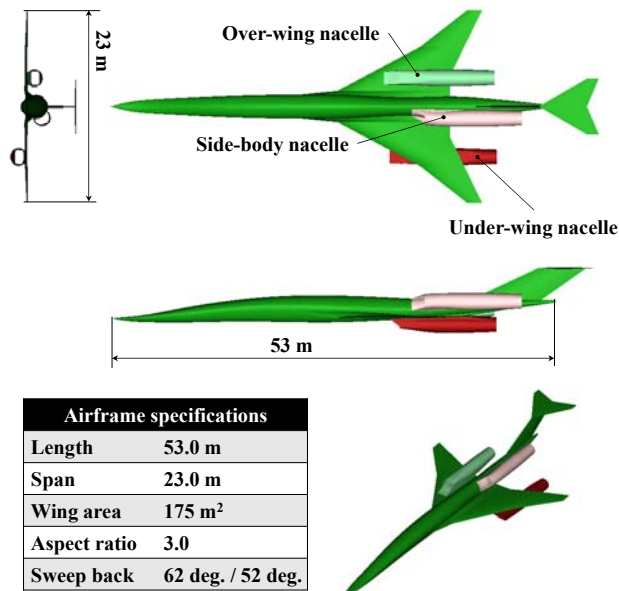


Fig. 1. Airframe and typical nacelle layout

The airframe shape was designed as JAXA's technical reference aircraft by applying its low-drag and low-boom design technology

(Fig. 1). Specifications of the engine were optimized to maximize range performance with the constraint of ICAO airport noise regulations [3]. The fan diameter is 1.7 m, the bypass ratio is 3.1, and the length including the nozzle is 6.4 m. The nozzle diameter at its exit was assumed to be the same as the fan diameter. Based on these specifications, the inlet and nacelle were designed by applying the method established at JAXA's silent supersonic technology demonstrator (S3TD) project [7]. The inlet is the two-stage external compression inlet. The typical inlet and nacelle shapes are shown in Fig. 2. Table 2 shows deviations from S3TD's inlet and nacelle. Main reasons to introduce these deviations were the followings: 1) The Mach number in front of the inlet depends on the nacelle position, and 2) The airframe shape to which the ramp is fitted depends on the nacelle position.

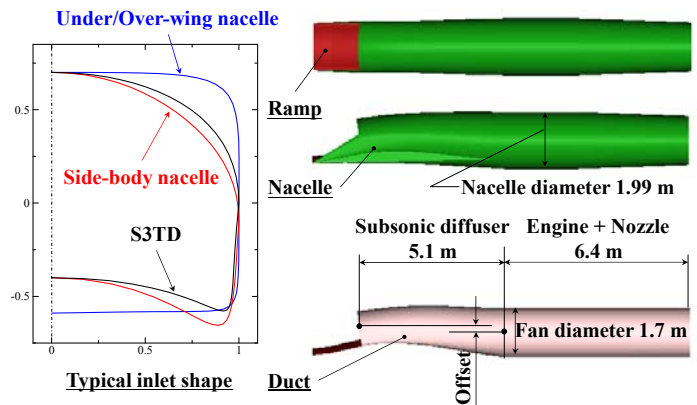


Fig. 2. Typical inlet and nacelle shape

Table 2. Comparison of inlet and nacelle shape

	S3TD	Present study
Supersonic diffuser		
1 st ramp	7 deg.	*1)
2 nd ramp	8 deg.	
Side wall	w/o side wall	w/ side wall
Inlet shape	Bezier curve	*2)
Subsonic diffuser		
Length over fan diameter	3.5	3.0
Offset over fan diameter	0.135	*3)

*1) The Mach number in front of the inlet is about 1.55 for under-wing nacelles and is about 1.65 for over-wing and side-body nacelles,

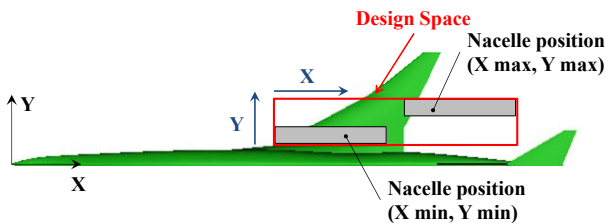
when the uniform flow Mach number is 1.6. The ramp angle was determined depending on the nacelle position so that the Mach number in front of the terminal shock is less than 1.3 to avoid the boundary layer separation behind the terminal shock.

*2) The frontal shape of the inlet was defined by the Bezier curve whose control points were placed depending on the nacelle position so that the ramp is fitted to the airframe shape.

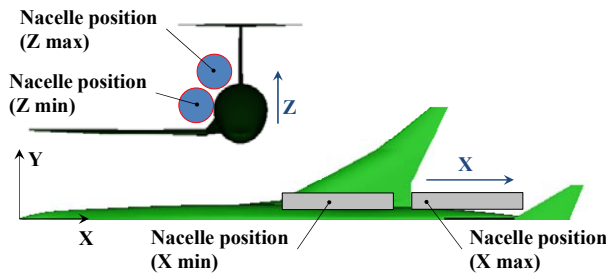
*3) The offset is the difference in the vertical position between centers of throat and engine (Fig. 2). For side-body nacelles, the offset was determined so that ramp and nozzle are fitted to the fuselage. For over-wing and under-wing nacelles, the offset was determined so that over-wing (under-wing) nacelles don't penetrate the lower (upper) surface of the wing. In this study, however, the offset was constrained to be less than 20% of the fan diameter to avoid large degradation of aerodynamic performance of the inlet. As a result, some over-wing nacelles penetrate the lower surface of the wing.

3 Definition of Optimization Problem

In the optimization study, the nacelle position (i.e., the position of center of throat) is the design variable.



(a) Over-wing and under-wing nacelle



(b) Side-body nacelle

Fig. 3. Design Space

The design space shown in Fig. 3 and Table 3 was defined without considering the feasibility of the structural design to see if a unique configuration can be optimum. For over-wing and under-wing nacelles, chord-wise and span-wise positions are design variables. For side-body nacelles, longitudinal and vertical positions are design variables.

Table 3. Design Space

Over & Under-wing		Side-body	
X min	28.514 m	X min	28.514 m
X max	41.508 m	X max	41.508 m
Y min	2.756 m	Z min	1.908 m
Y max	6.360 m	Z max	2.332 m

The lift-to-drag ratio and the sonic boom intensity are the objective functions, which were evaluated by JAXA's tools at the design condition (Mach number=1.6, CL=0.15, and altitude=14.6 km). Regarding the sonic boom intensity, the difference from the glider configuration (i.e., airframe alone) is the index.

The lift-to-drag ratio was evaluated by the Euler analysis using JAXA's FaSTAR code [8] and the empirical relation for the skin friction drag [9]. In the Euler analysis, the unstructured grid was used. The number of cells was approximately 2×10^7 . The SLAU scheme was applied to the advection term and the LU-SGS method was used for the implicit time integration. As for the propulsion system, the nacelle was modeled as the through-flow nacelle. The lift coefficient includes the aerodynamic force of both nacelle and ramp (Fig. 2). On the other hand, the drag coefficient includes only the aerodynamic force of the nacelle, because the drag acting on the ramp is regarded as the loss of thrust that is taken into account in the propulsion system.

In the evaluation of the sonic boom intensity, the FaSTAR code was again used to perform the Euler analysis. The same scheme as described above was applied, however, the number of cells was increased to about 5×10^7 in order to reduce the dissipation. The near-field pressure distributions were extracted on the cylinder surface (Fig. 4). These pressure distributions were modified by the multi-pole analysis [10] to take into account the

propagation in the circumferential direction. Then, the far-field propagation analysis based on the Burgers equation [11] was performed to obtain the sonic boom signature on the ground. The reflection factor on the ground was 1.9. The sonic boom intensity was evaluated in PLdB.

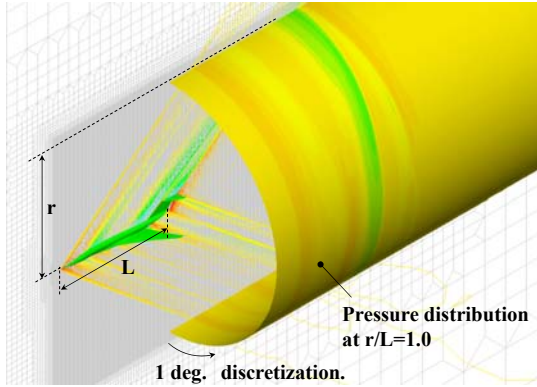


Fig. 4. Evaluation of sonic boom

The computation cost as well as the fidelity of these analyses is high. In this study, the response surface (i.e., the Kriging model [12]) was constructed to reduce the computation cost. Firstly, the response surface was constructed with 8 initial samples. Then, several samples were added considering the probability of improvement until the Pareto front came close to samples.

4 Results and Discussion

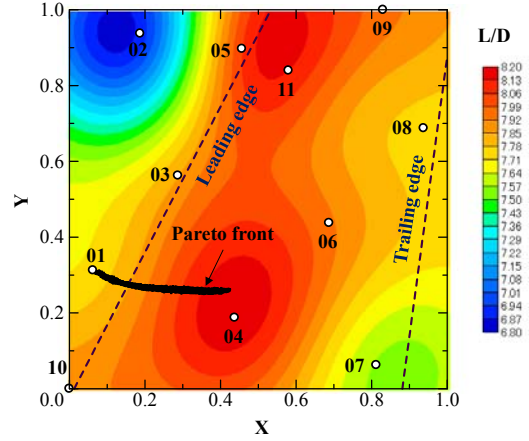
4.1 Pareto optimal solutions

In this section, the characteristics of response surfaces of L/D and sonic boom intensity are discussed. Then, the Pareto optimal solutions are compared between three nacelle layouts.

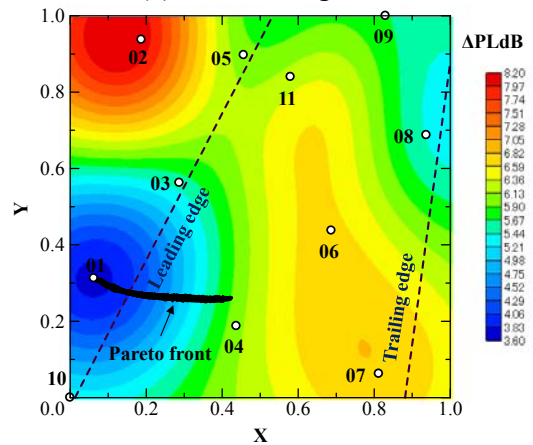
Under-wing nacelle:

The response surface of the under-wing nacelle (UWN) is shown in Fig. 5. The x and y axes are normalized by the width of the design space in the correspondent directions. The numbers shown in Fig. 5 correspond to sample numbers. For example, “01” is referred to as “UWN01”. The Pareto optimal solutions with respect to L/D and sonic boom intensity are plotted in Fig. 5. The response surface of the angle of attack

(AoA) is not shown. In all samples, AoA is smaller than that of the glider configuration (3.1 deg.), because the nacelle shock wave acts as a compression lift.



(a) Lift-to-drag ratio



(b) Sonic boom

Fig. 5. Response surface of UWN

The breakdown of the drag coefficient is shown in Fig. 6 to see the effect of the nacelle position on L/D.

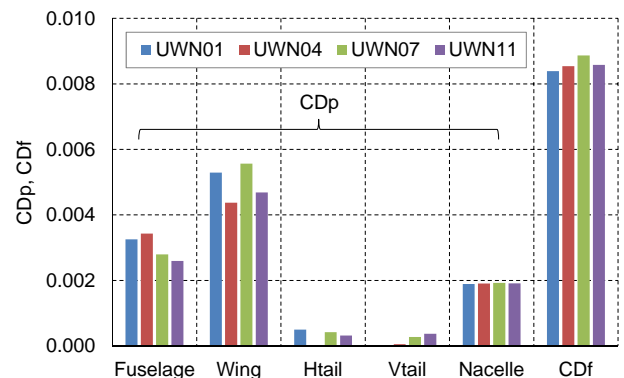


Fig. 6. Breakdown of drag coefficient of UWN

Firstly, the effect of the chord-wise nacelle position is discussed based on the results of UWN01, UWN04, and UWN07. The largest difference between these samples can be seen at the wing pressure drag. In UWN01, the ramp is placed in front of the wing leading edge, and the nacelle shock wave acts on the front part of the wing (Fig. 7), which causes large wing drag. In UWN04, most of the nacelle shock wave acts as a compression lift, which results in the smallest AoA. Moreover, the nacelle shock wave acts on the rear part of the wing and decreases wing pressure drag along with the smallest AoA. As a result, UWN04 shows the largest L/D among all samples including side-body and over-wing nacelles. In UWN07, there is almost no contribution of the nacelle shock wave to the compression lift, and AoA is the largest, which increases wing pressure drag. In addition, the large wetted area of the nacelle is another reason to decrease L/D. Consequently, the contribution of the nacelle shock wave to both increase in lift and decrease in drag is important in determining the chord-wise nacelle position. To achieve this contribution, the nacelle should be placed at the intermediate chord of the wing (about 35% chord in this study).

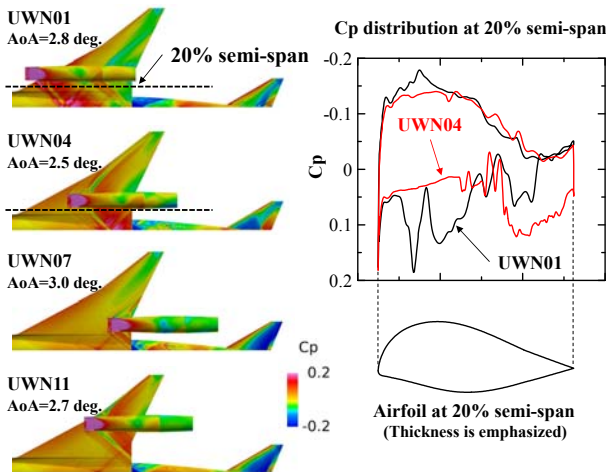


Fig. 7. Surface pressure distribution of UWN

The span-wise nacelle position is discussed based on UWN04 and UWN11. The drags of fuselage and tails are different between two samples (Fig. 6) because the interaction of the nacelle shock wave with these parts is different. However, the difference in the total pressure drag is only 1 drag count. Thus, the span-wise

nacelle position has little impact on L/D, and the chord-wise nacelle position should be emphasized in determining the nacelle position.

The sonic boom signature on the ground is shown in Fig. 8 to examine the effect of the nacelle position on the sonic boom intensity.

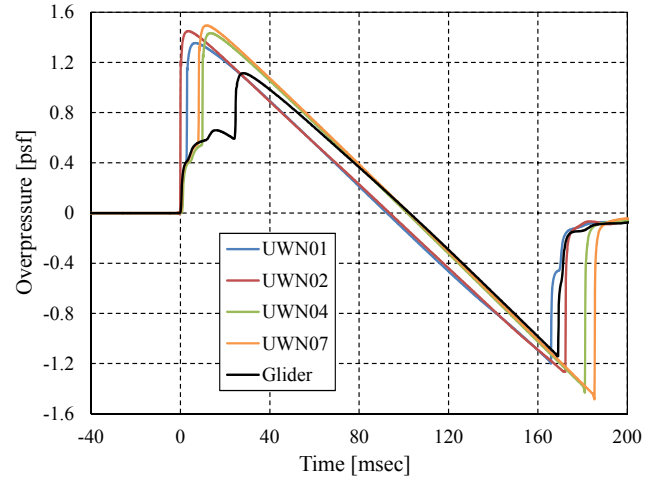


Fig. 8. Sonic boom signature of UWN

In UWN01, the ramp is placed in front of the wing leading edge. The ramp and wing shock waves are merged as they propagate toward the ground. The overpressure caused by the merged shock wave (i.e., the second shock wave of the front boom) is larger than that of the glider configuration. The merged shock wave, however, does not merge with the nose shock wave. On the other hand, in UWN02, the front part of the nacelle that is placed in front of the wing leading edge causes stronger second shock wave, which is merged with the nose shock wave on the ground. As a result, UWN02 shows the single overpressure at the front boom, which leads to the strongest sonic boom intensity. Regarding the rear boom, its intensity is affected by the nacelle expansion wave. In UWN07, the expansion wave can be observed at the rear part of the nacelle (Fig. 9). In UWN01, however, this expansion wave can't be seen, because the rear part of the nacelle is covered with the wing and the expansion from the lower surface to the upper surface of the nacelle is kept weak. The weak expansion at the rear part of the nacelle along with small AoA due to the compression lift results in the two-stage overpressure at the rear boom (Fig. 8), while the

glider configuration shows nearly single overpressure at the rear boom. Consequently, UWN01 realizes the weakest sonic boom intensity among under-wing nacelles due to the reduced rear boom even though it causes strong front boom. When the nacelle is placed behind UWN01, for example in UWN04, the expansion at the rear part of the nacelle becomes strong (Fig. 9) and the rear boom shows single overpressure. In UWN07, the compression lift due to the nacelle shock wave is small. The larger AoA contributes to the larger sonic boom intensity than that of UWN04.

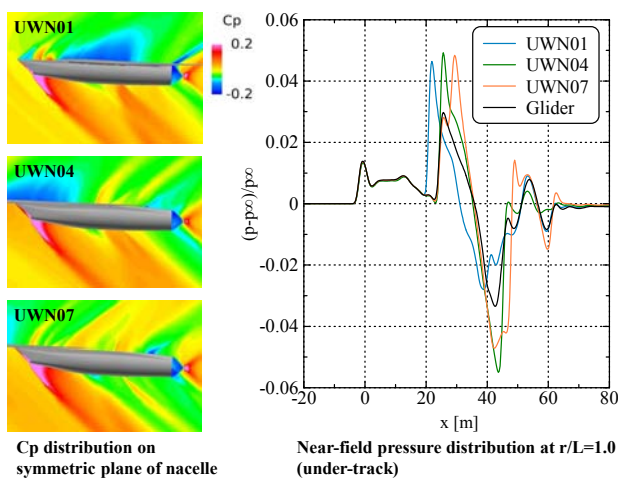


Fig. 9. Spatial pressure distribution of UWN

Based on the above discussion, it is important in determining the nacelle position to reduce the expansion at the rear part of the nacelle in order to reduce the sonic boom intensity, which is realized in UWN01 by placing the rear part of the nacelle under the wing. At the same time, it should also be noted that the nacelle shock wave does not merge with the nose boom.

Finally, the nacelle position is discussed from viewpoints of both low-drag and low-boom. The Pareto front shown in Fig. 5 includes UWN01 that realizes the weakest sonic boom intensity. When the nacelle is placed behind UWN01, the nacelle shock wave decreases the wing pressure drag. Thus, the Pareto front appears behind UWN01. This result shows the importance of the chord-wise nacelle position in the tradeoff between low-drag and low-boom. The key point in determining the chord-wise nacelle position is to consider both the drag reduction using the nacelle shock wave and the

boom reduction by reducing the expansion at the rear part of the nacelle.

Side-body nacelle:

The response surface of the side-body nacelle (SBN) is shown in Fig. 10. The response surface of AoA is not shown, but AoA is larger than that of the glider configuration, because the nacelle shock wave decreases lift as explained later.

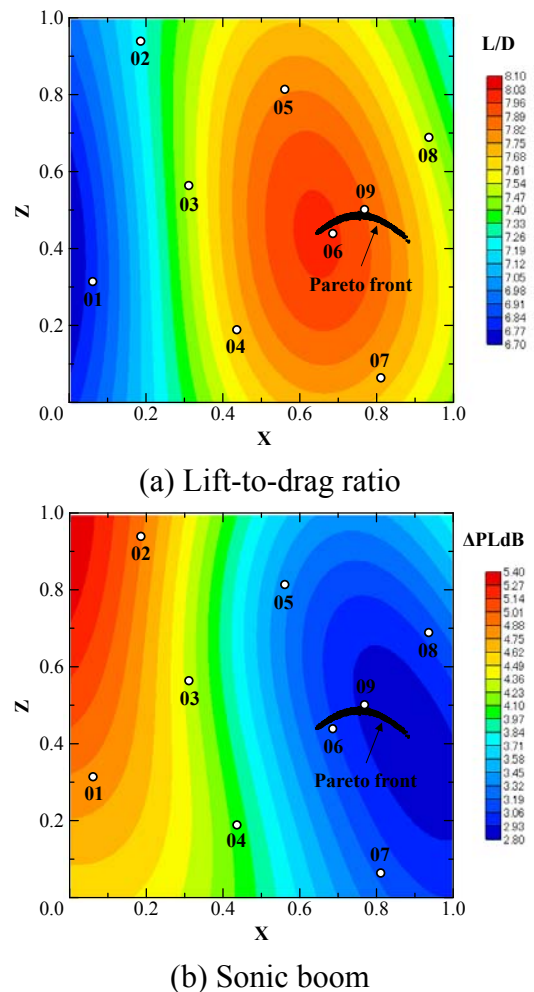


Fig. 10. Response surface of SBN

The lift-to-drag ratio depends mainly on the longitudinal nacelle position. To show the effect of the longitudinal nacelle position on L/D, the surface pressure distribution is shown in Fig. 11. In the same manner as under-wing nacelles, the wing pressure drag depends on how the nacelle shock wave acts on the wing surface. Among these samples shown in Fig. 11, SBN04 shows the smallest wing pressure drag. On the other hand, in contrast to under-wing

nacelles, the nacelle shock wave decreases lift and increases AoA. In SBN04, the wing pressure drag is the smallest, however, the large AoA increases the fuselage pressure drag. As a result, SBN06 that shows the second smallest wing pressure drag realizes larger L/D than that of SBN04 due to smaller AoA. In SBN08, the nacelle shock wave does not reduce the wing pressure drag and its L/D is smaller than that of SBN06. Thus, SBN06 in which the nacelle shock wave acts on around the wing trailing edge realizes the largest L/D among side-body nacelles. The longitudinal nacelle position should be determined so that the nacelle shock wave reduces the wing pressure drag while reducing its negative effect of the decrease in lift. Regarding the vertical nacelle position, its effect on L/D is small (Fig. 10), but the intermediate position is appropriate to reduce the interference of the nacelle with wing, vertical and horizontal tails.

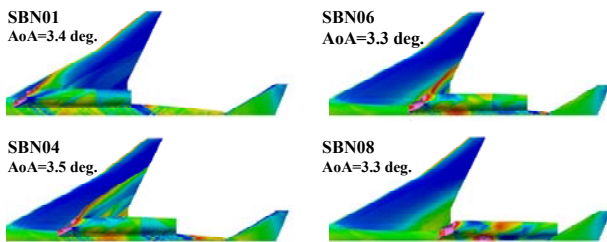


Fig. 11. Surface pressure distribution of SBN

The sonic boom signature on the ground is shown in Fig. 12 to explain the effect of the nacelle position on the sonic boom intensity.

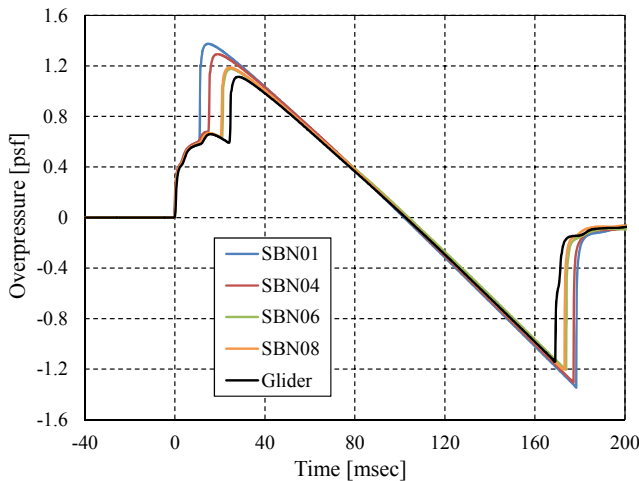


Fig. 12. Sonic boom signature of SBN

Most of the nacelle shock wave is shielded by the wing (Fig. 11), and therefore, its effect on the sonic boom intensity is small. In SBN08, the nacelle shock wave is not shielded (Fig. 11), but it propagates mainly in the lateral direction and its propagation toward the ground is prevented by the fuselage. Thus, the effect of the nacelle shock wave is still small in SBN08. As a result, the sonic boom intensity depends largely on AoA. As the longitudinal nacelle position goes backward, the negative lift produced by the nacelle shock wave becomes small, which reduces the sonic boom intensity.

From viewpoints of both low-drag and low-boom, the Pareto front (Fig. 10) shows the importance of the longitudinal nacelle position. As discussed above, when the nacelle is placed at the rear part of the design space, the sonic boom intensity becomes weak due to smaller AoA, while L/D becomes small due to less drag reduction by the nacelle shock wave. Consequently, the key point in determining the longitudinal nacelle position is to obtain the optimum compromise between increase in AoA and decrease in the wind drag, both of which are caused by the nacelle shock wave.

Over-wing nacelle:

The response surface of the over-wing nacelle (OWN) is shown in Fig. 13. The response surface of AoA is not shown, but AoA is larger than that of the glider configuration in the same manner as side-body nacelles.

The lift-to-drag ratio depends mainly on the chord-wise nacelle position. The nacelle shock wave acts on the wing upper surface in the same manner as side-body nacelles. Thus, the key point in determining the chord-wise nacelle position considering L/D alone is the same as that of side-body nacelles. In this study, the largest L/D is achieved at about 65% chord, which is behind that of the under-wing nacelle (35% chord). In under-wing nacelles, the nacelle shock wave is beneficial to both lift and drag, while it has negative effect on lift in over-wing nacelles. To improve L/D, therefore, the interaction of the nacelle shock wave with the wing should be reduced in over-wing nacelles compared to under-wing nacelles. As a result, the chord-wise nacelle position to realize the

maximum L/D is behind that of under-wing nacelles. The lateral nacelle position slightly affects the pressure drag of fuselage and tails in the same manner as under-wing nacelles, but it has less impact on L/D than the chord-wise position.

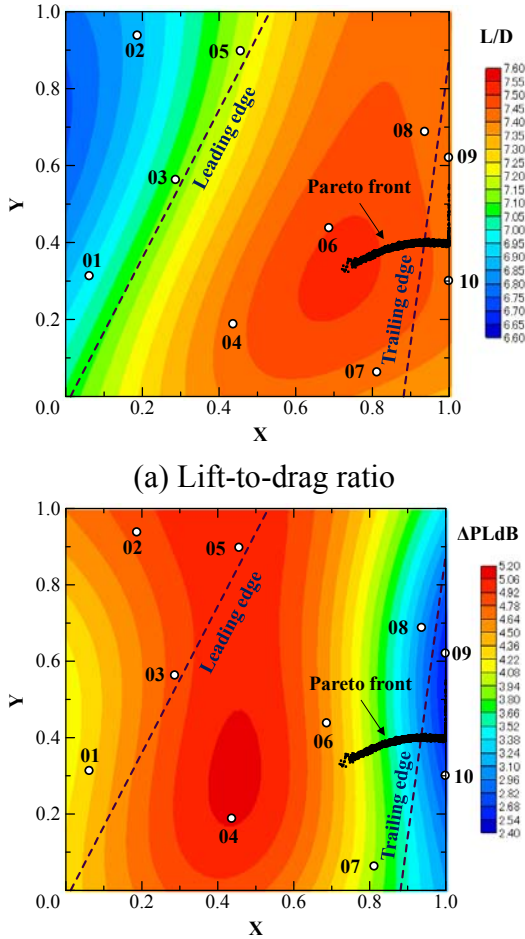


Fig. 13. Response surface of OWN

The sonic boom signature on the ground is shown in Fig. 14 to explain the effect of the nacelle position on the sonic boom intensity. When the ramp is placed on the wing upper surface, most of the nacelle shock wave is shielded by the wing, and the sonic boom intensity depends mainly on AoA. In OWN04 of which AoA is the largest (3.7 deg.), strong front and rear booms are observed. When the ramp is placed in front of the wing leading edge (e.g., OWN01), the ramp shock wave propagates toward the ground, which causes almost the same front boom intensity as that of OWN04, even though AoA (3.2 deg.) is smaller

than that of OWN04. When the ramp is placed at the rear part of the wing (e.g., OWN07 and OWN09), the negative lift caused by the nacelle shock wave is small. Small AoA results in the weak sonic boom intensity. In OWN07 and OWN09, AoAs are the same (3.3 deg.), however, OWN09 shows smaller overpressure at the rear boom. In OWN09, the nacelle shock wave is spilled from the wing trailing edge and propagates toward the ground, which reduces the expansion at the rear part of the vehicle (Fig. 15). As a result, OWN09 realizes the weakest sonic boom intensity. Thus, in order to reduce the sonic boom intensity, the nacelle should be placed at the rear part of the wing to reduce the AoA and to utilize the nacelle shock wave.

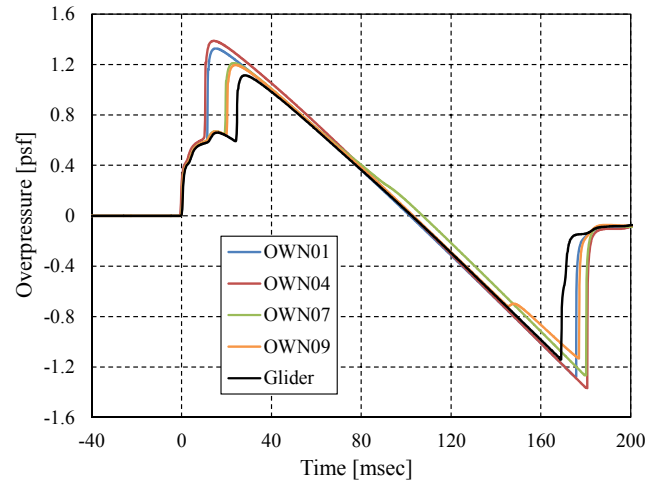


Fig. 14. Sonic boom signature of OWN

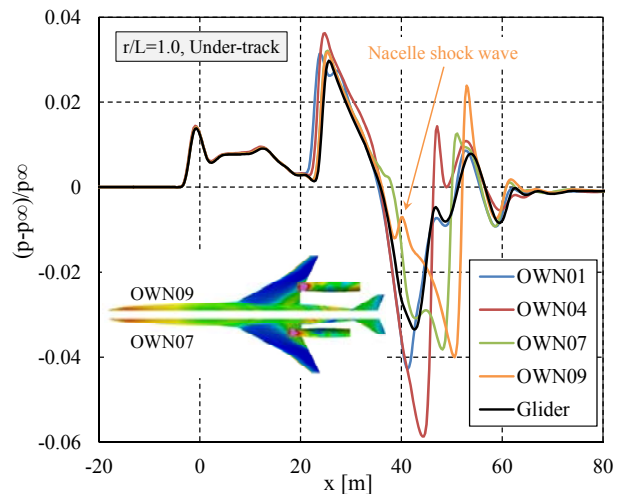


Fig. 15. Near-field pressure signature of OWN

From viewpoints of both low-drag and low-boom, the chord-wise nacelle position is

important. When the nacelle is placed at the intermediate wing chord, the nacelle shock wave reduces drag. When the nacelle is placed at the rear part of the wing, the nacelle shock wave reduces sonic boom. Thus, it is important in determining the chord-wise position to find the optimum compromise between these benefits from the nacelle shock wave.

Comparison of Pareto optimal solutions:

The Pareto fronts of three nacelle layouts are shown in Fig. 16.

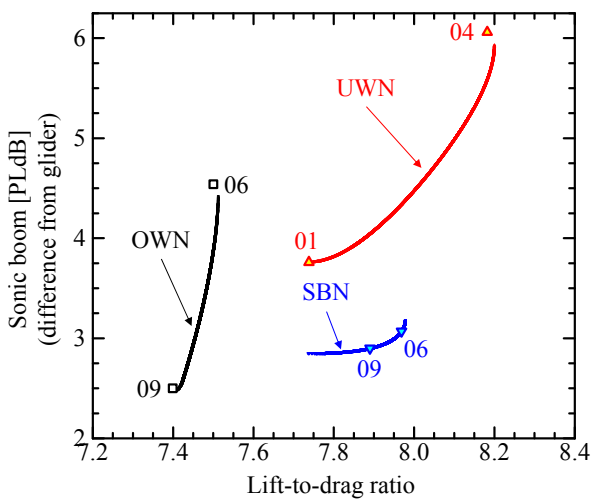


Fig. 16. Pareto optimal solutions

The under-wing nacelle shows large L/D because the nacelle shock wave produces the compression lift and reduces the wing pressure drag. The nacelle shock wave, however, propagates toward the ground and causes strong front boom. On the other hand, in the over-wing nacelle, the nacelle shock wave can be utilized to reduce the rear boom intensity, when the nacelle is placed at the rear part of the wing. However, the negative lift caused by the nacelle shock wave reduces L/D. The wing covered with the nacelle whose aerodynamic performance is poor is another reason for the small L/D. The side-body nacelle overcomes these drawbacks. The drawback of the under-wing nacelle is overcome by shielding the nacelle shock wave by fuselage and wing. The drawback of the over-wing nacelle is overcome by enlarging the distance between nacelle and wing to reduce the negative lift. Moreover, the wing upper surface is not covered with the

nacelle, and produces its original aerodynamic performance. Consequently, the side-body nacelle realizes the optimum compromise between L/D and sonic boom intensity.

4.2 Design guides

The side-body nacelle should be selected out of three nacelle layouts examined here in order to obtain the optimum compromise between L/D and sonic boom intensity. The design guides for the side-body nacelle is summarized in Fig. 17.

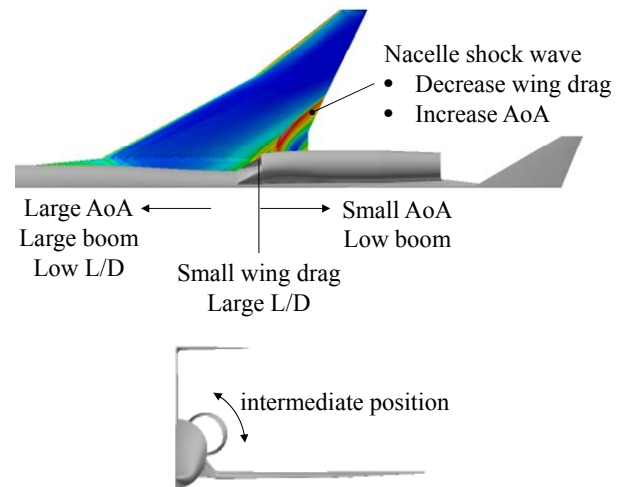


Fig. 17. Design guides for SBN

Longitudinal position: Since the nacelle shock wave has little impact on the sonic boom intensity, it is important to reduce AoA in order to realize low-boom. Thus, the nacelle should be placed at the rear part of the fuselage so that the nacelle shock wave does not act on the wing upper surface. On the other hand, the nacelle shock wave acting on the wing upper surface reduces the wing pressure drag. From the L/D point of view, the nacelle should be placed slightly ahead of the wing trailing edge. It should be noted that the nacelle shock has the negative effect of increasing both AoA and wing pressure drag when its interaction with the wing upper surface is too large. As discussed above, low-drag and low-boom are conflicting. Thus, the optimum compromise between low-drag and low-boom should be achieved considering the effect of the nacelle shock wave.

Vertical position: The intermediate vertical position is appropriate to reduce the interference

of the nacelle with wing, vertical and horizontal tails.

5 Conclusions

The integration of a propulsion system with an airframe for a supersonic transport was examined from viewpoints of both low-drag and low-boom. The nacelle position was optimized for three types of nacelle layout, and design guides were discussed.

Results show that the interference between nacelle shock wave and wing has a large impact on both low-drag and low-boom. In under-wing nacelles, the nacelle shock wave increase both L/D and sonic boom intensity. In over-wing nacelles, the weakest sonic boom intensity is realized by utilizing the nacelle shock wave, however, aerodynamic performance of the wing is degraded by the nacelle, which results in small L/D. The side-body nacelle realizes the optimum compromise between low-drag and low-boom by utilizing the nacelle shock wave. In side-body nacelles, the longitudinal nacelle position has a larger impact on both low-boom and low-drag than the vertical nacelle position. The key point in determining the longitudinal position is to obtain the optimum compromise between increase in the angle of attack and decrease in the wind drag, both of which are caused by the nacelle shock wave.

Acknowledgements

The author would like to express its appreciation for the technical support provided by people from Applied Aerodynamics Department of the French Aerospace Lab (ONERA).

References

- [1] Murakami A. Research Activities on Supersonic Technology at JAXA. *The 2010 Asia-Pacific International Symposium on Aerospace Technology*, 2010.
- [2] Honda M and Yoshida K. D-SEND Project for Low Sonic Boom Design Technology. *28th Congress of the International Council of the Aeronautical Sciences*, 2012.
- [3] Ueno A, Watanabe Y, and Asako T. Conceptual Design of Silent Supersonic Transport Considering Airframe/Propulsion Integration. *50th Aircraft Symposium*, 2012. (in Japanese)
- [4] Morgenstern J et al. Advanced Concept Studies for Supersonic Commercial Transports Entering Service in the 2018 to 2020 Period, Phase I Final Report. NASA/CR-2013-217820, 2013.
- [5] Magee T, Shaw S, and Fugal S. Experimental Validations of a Low-Boom Aircraft Design. *51st AIAA Aerospace Sciences Meeting including the New Horizons Forum and Aerospace Exposition*, AIAA 2013-0646, 2013.
- [6] Ordaz I and Li W. Adaptive Aft Signature Shaping of a Low-Boom Supersonic Aircraft Using Off-Body Pressures. *50th AIAA Aerospace Sciences Meeting including the New Horizons Forum and Aerospace Exposition*, AIAA 2012-0020, 2012
- [7] Watanabe Y, Ueno A, and Murakami A. Design of Top Mounted Supersonic Inlet for Silent Supersonic Technology Demonstrator S3TD. *27th Congress of the International Council of the Aeronautical Sciences*, 2010.
- [8] Hashimoto A et al. Toward the Fastest Unstructured CFD Code 'FaSTAR'. *50th AIAA Aerospace Sciences Meeting including the New Horizons Forum and Aerospace Exposition*, AIAA 2012-1075, 2012
- [9] Raymer D. P. *Aircraft Design: A Conceptual Approach*, 4th edition, AIAA Education Series, AIAA, 2006
- [10] Kanamori M et al. Improvement of Near-field Waveform from Supersonic Vehicle Using Multipole Analysis. JAXA-SP-13-011, 2013. (in Japanese)
- [11] Yamamoto M et al. Long-range Sonic Boom Prediction Considering Atmospheric Effects. *Inter-noise 2011*, 2011.
- [12] Simpson T et al. Comparison of Response Surface and Kriging Models for Multidisciplinary Design Optimization. *7th AIAA/USAF/NASA/ISSMO Symposium on Multidisciplinary Analysis and Optimization*, AIAA 98-4755, 1998.

Copyright Statement

The authors confirm that they, and/or their company or organization, hold copyright on all of the original material included in this paper. The authors also confirm that they have obtained permission, from the copyright holder of any third party material included in this paper, to publish it as part of their paper. The authors confirm that they give permission, or have obtained permission from the copyright holder of this paper, for the publication and distribution of this paper as part of the ICAS 2014 proceedings or as individual off-prints from the proceedings.